Signal Processing 172 (2020) 107562

Contents lists available at ScienceDirect

Signal Processing

journal homepage: www.elsevier.com/locate/sigpro

Rate-distortion model for grayscale-invariance reversible data hiding

Siyan Zhou[a], Weiming Zhang[b], Chaomin Shen[a,*]

[a] Shanghai Key Laboratory of Multidimensional Information Processing, School of Computer Science, East China Normal University, Shanghai, China
[b] School of Information Science and Technology, University of Science and Technology of China, Hefei, China

ARTICLE INFO

Article history:
Received 16 December 2019
Revised 16 February 2020
Accepted 1 March 2020
Available online 2 March 2020

Keywords:
Grayscale invariance
Rate-distortion model
Optimal modification
Recursive code construction
Reversible data hiding

ABSTRACT

Recently, a novel scheme called grayscale-invariance reversible data hiding (RDH) has been developed, in which the generated color marked image will have the same grayscale as that of the host color image. Due to the property of grayscale invariance, for many cases, the further applications and image processing of the marked image will not be interfered with. However, the performance of current grayscale-invariance RDH is unsatisfactory, and the corresponding theoretical model is also lacking. For grayscale-invariance RDH, the modifications of the three color channels are interrelated. By decomposing the joint modification and associating the modification distortions of the green scales and blue scales with those of the red scales, we first approximate the modification-independent rate-distortion model for grayscale-invariance RDH. Subsequently, the optimal transition probability matrix can be estimated, according to which we implement the theoretically proven optimal modification, i.e., recursive code construction (RCC), to finish message embedding. The experimental results show that the presented method extends the applications of RCC and can significantly improve the performance of grayscale-invariance RDH.

1. Introduction

Reversible data hiding (RDH) is a special type of data hiding, whereby both the host signal and the embedded data can be restored from the marked signal without loss. Such technology is typically used for data annotation of highly valuable files, such as medical [1], military and judicial files [2], where minor modifications are not allowed. Recently, studies have shown that RDH may have various valuable applications including image authentication and self-recovery [3], covert storage [4,5], medical and military image processing [6], video error-concealment coding [7,8], multimedia archive management [9], image transcoding [10], data coloring in the cloud [11], and so on.

Many RDH algorithms have been proposed in the past decade, usually consisting of two steps. The first step is to generate a sequence with a histogram that is as steep as possible. For an image, the prediction errors (PEs) of pixels are the most commonly used host sequence. The second step is to reversibly modify the host sequence to finish message embedding by introducing as little distortion as possible. Based on the modification manner, RDH can be classified into three fundamental strategies: difference expansion [12–19], histogram shift [20–25] and recursive code construction (RCC) [5,26–31].

Due to the modification, compared to the original host image, the generated marked image will be deemed a noisy image, and thus, its further processing will be interfered with. Taking Fig. 1(a) as an example, after message embedding, we match the marked image and the host image based on scale invariant feature transform (SIFT) descriptors, giving rise to occurrence of false SIFT matches. In many cases, especially for medical and military image processing, the decrease in processing accuracy may be disappointing. Of course, the host image can be losslessly restored from the marked image and then is free for any further processing. However, in addition to the computation cost for recovery, the embedding algorithm and secret key are both mastered by the steganographer, so it is nearly impossible for the processors to restore the host image prior to each processing. Indeed, the processors even cannot understand whether or not the input image is a marked image.

Therefore, RDH that does not affect further processing of the marked image is desired. Hou et al. [33] observe that transforming a color image into a gray image is rather general in practical application because the computational cost of gray image processing is strongly reduced compared to that of color image processing. Some algorithms even only operate on the luminance channel of a color image such as the well-known Haar-like descriptors [35], histogram of oriented gradients (HOG) descriptors [36], SIFT descriptors [37], and almost all of their applications. Therefore, many

* Corresponding author.
E-mail addresses: 51184506084@stu.ecnu.edu.cn (S. Zhou), zhangwm@ustc.edu.cn (W. Zhang), cmshen@cs.ecnu.edu.cn (C. Shen).

https://doi.org/10.1016/j.sigpro.2020.107562
0165-1684/

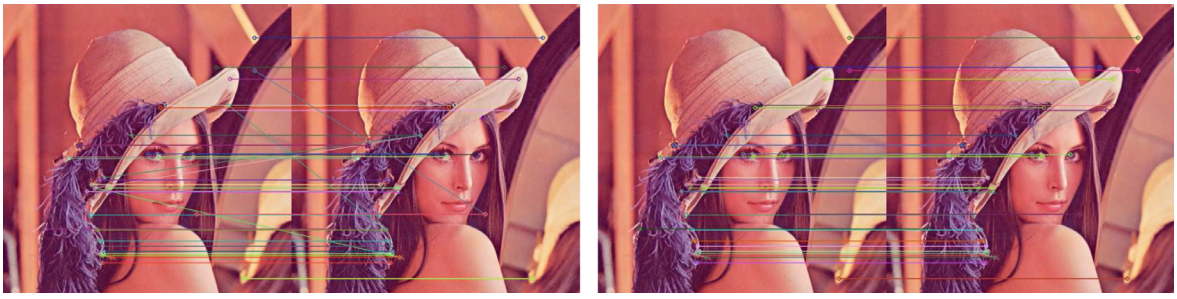

(a) Embedding 260,000 bit messages with Ou *et al.*'s method [32].

(b) Embedding 260,000 bit messages with Hou *et al.*'s method [33].

Fig. 1. SIFT matching between the host image and marked image.

algorithms convert a color image into a gray version and then operate on the latter. For this reason, Hou et al. propose grayscale-invariance RDH [33] that embeds messages into the color image without changing the corresponding grayscale.

For grayscale-invariance RDH, as long as the current pixel (including three scales in red, green and blue channels) is modified, it will yield a one-bit error correction message for recovery. Using Hou et al.'s method [33], each red scale accommodates a one-bit secret message, and each blue scale accommodates a one-bit error correction message; correspondingly, the green scale is adaptively adjusted to keep the grayscale unchanged. It is clear that each pixel can only carry a one-bit secret message with the three scales being modified, resulting in a low embedding efficiency. Later, Gao et al. [34] enlarge the embedding capacity by adaptive embedding pattern. However, the distortion controls are unsatisfactory in the existing schemes due to the lack of the optimal strategy.

Indeed, in the field of RDH, RCC is a modification method that originated from studying the bound of a rate-distortion model [26] formulated as:

$$\begin{aligned} \min \quad & \sum_{x=0}^{m-1}\sum_{y=0}^{n-1} P_X(x)P_{Y|X}(y|x)d(x,y) \\ \text{s.t.} \quad & H(\mathbf{Y}) = \rho + H(\mathbf{X}) \end{aligned}, \tag{1}$$

where $P_X(x)$ is the probability distribution of host sequence $\mathbf{X}$, $d(x, y)$ is the distortion metric for modifying x to y, $P_{Y|X}(y|x)$ is the transition probability matrix, and ρ is the embedding rate. As observed from Eq. (1), to realize the optimal modification, we must first solve the optimal transition probability matrix (OTPM). Based on the OTPM, many RCC schemes have been developed, among which recursive histogram modification (RHM) [29] has been proved to reach the rate-distortion bound in both experiment and theory.

An OTPM implying the optimal modification of host sequence is essential to coding and decoding processes of RCC schemes. For consistent distortion metrics, the solutions of the OTPM are summarized in [30,31], and for inconsistent distortion metrics, we can also find the corresponding solutions in [5]. However, all existing solutions are based on the assumption that the modifications of different elements are independent. For grayscale-invariance RDH, the green channel is adaptively adjusted according to the modifications of the red and blue channels, and the modified indices of blue scales are determined by the modifications of red scales. That is, while the modifications of the three color channels are interrelated, the existing RCC schemes cannot be applied to solve modification-dependent optimization.

For the grayscale-invariance scheme, the natural problem is to develop the rate-distortion model and a method for its solutions. By analyzing the interrelation among the red, green and blue channels, we define the joint modification cost for the red, green and blue channels and give the rate-distortion model for grayscale-invariance RDH. To solve this rate-distortion model, we build the associations between the modification distortions of the green and blue scales and those of the red scales. Thus, the modification-dependent model is estimated with a modification-independent model, and then, the corresponding OTPM can be solved by the existing algorithms. The OTPM implies the optimal modification approach, based on which we implement RHM to finish message embedding. By the proposed model, both the capacity and the rate-distortion curve of the grayscale-invariance RDH can be significantly improved.

The rest of the paper is organized as follows. We introduce related works in Section 2. Section 3 introduces separable grayscales for prediction and elaborates the presented rate-distortion model for grayscale-invariance RDH. The experimental results are given in Section 4 to demonstrate the advantages of our method relative to the previous methods. Finally, the paper is concluded with a discussion in Section 5.

2. Related works

Throughout the paper, matrices and vectors are denoted by boldface fonts. We denote the host sequence as $\mathbf{X}$ with its elements belonging to $\mathcal{X} = \{0, 1, \cdots, m-1\}$, and the marked sequence as $\mathbf{Y}$ with its elements belonging to $\mathcal{Y} = \{0, 1, \cdots, n-1\}$. A pixel consists of three scales {*r*, *g*, *b*}, and host sequence means the PEs of selected host scales for accommodating messages.

2.1. Hou et al.'s grayscale-invariance RDH

The most widely used algorithm for converting a color image to the corresponding gray image is described by

$$f_{c2v}(r, g, b) = \lfloor 0.299r + 0.587g + 0.114b \rceil, \tag{2}$$

where $\lfloor x \rceil$ rounds the element x to its nearest integer, and *r*, *g*, *b* are scales from the red, green, and blue channels, respectively.

Different from all of the previous color RDH algorithms [32,38–43] pursuing a high peak signal-to-noise ratio (PSNR), after embedding messages through modifying {*r*, *b*} to {r', b'}, Hou et al. [33] adaptively adjust g to g' to keep grayscale v unchanged by using

$$g' = f_{v2g}(r', b', v) = \lfloor (v - 0.299r' - 0.114b')/0.587 \rceil. \tag{3}$$

Of course, by Eq. (3) we obtain

$$f_{c2v}(r, g, b) = f_{c2v}(r', g', b') = v. \tag{4}$$

At the receiver's end, {*r*, *b*} can be restored from {r', b'} after extracting the embedded messages, combined with the unchanged grayscale v, and g can be roughly calculated as

$$g^c = f_{v2g}(r, b, v). \tag{5}$$

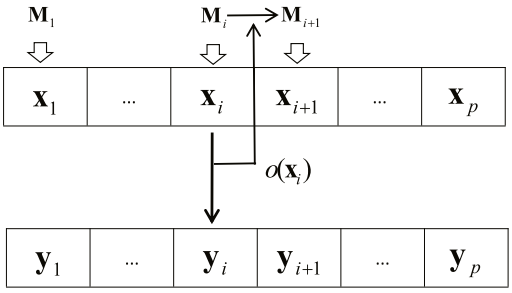

Fig. 2. Recursive embedding of RHM.

There may exist an offset between g^c and g due to the round function, but the magnitude of such offset can be only 1 or 0 because the weight of the green scale is more than 0.5. To restore the green scale exactly, we need one-bit error correction message to record the offset, denoted by m^c, as

$$m^c = |g - f_{v2g}(r, b, v)|. \tag{6}$$

m^c represents the magnitude of the offset between g^c and g so that $g = g^c + 1$ or $g = g^c - 1$. Since the weight of the green scale is more than 0.5, there must exist $f_{v2g}(r, g^c + 1, b) \neq v$ or $f_{v2g}(r, g^c - 1, b) \neq v$, and only the true one will keep v unchanged. Therefore, with the help of m^c, the receiver can exactly restore g according to r, b, v, and g^c.

2.2. Recursive code construction

For RDH, we embed L-bit messages into the host sequence $\mathbf{X} = (x_1, \cdots, x_N)$ by slightly modifying its elements to yield the marked sequence $\mathbf{Y} = (y_1, \cdots, y_N)$. The average distortion between $\mathbf{X}$ and $\mathbf{Y}$ under the embedding rate ρ ($\rho = L/N$) should be as small as possible.

After obtaining the rate-distortion bound in Eq. (1), researchers naturally hope to find the optimal embedding method minimizing the embedding distortion, that is, the optimal coding. It is observed from the model Eq. (1) that the OTPM implies the optimal modification of the host sequence. Based on the OTPM, many RCC schemes have appeared, among which Zhang et al.'s RHM [29] has been proven to reach the rate-distortion bound in both experiment and theory, whose core idea is as follows.

Prior to embedding, we first divide the host sequence $\mathbf{X} = (x_1, \cdots, x_N)$ into p subsequences denoted by $\mathbf{x}_i$, $1 \leq i \leq p$. For $\mathbf{x}_i$, the messages $\mathbf{M}_i$ are decoded according to the OTPM $P_{Y|X}(y|x)$ to generate the marked subsequences $\mathbf{y}_i$, and then, $\mathbf{x}_i$ is compressed as $O(\mathbf{x}_i)$ according to the OTPM $P_{X|Y}(x|y)$. Note that the OTPM $P_{Y|X}(y|x)$ from $\mathbf{X}$ to $\mathbf{Y}$ and the OTPM $P_{X|Y}(x|y)$ from $\mathbf{Y}$ to $\mathbf{X}$ can be mutually converted. $O(\mathbf{x}_i)$ is added to the remaining $\mathbf{M}_i$ to form a new message stream $\mathbf{M_{i+1}}$ for the next subsequence to embed. Because the entropy of $P_{Y|X}(y|x)$ is higher than that of $P_{X|Y}(x|y)$, the volume of consumed message stream for generating $\mathbf{y}_i$ is larger than $O(\mathbf{x}_i)$. Thus, the secret messages can be embedded subsequence by subsequence, and the capacity of each $\mathbf{x}_i$ is the reduced volume from $\mathbf{M_i}$ to $\mathbf{M_{i+1}}$. The recursive embedding diagram of RHM is shown in Fig. 2, and the reader is referred to [29] for the details.

RHM is one of the optimal modification methods that is based on the OTPM. For consistent distortion metrics, the solutions of the OTPM are summarized in [30,31], and for inconsistent distortion metrics, we can also find the corresponding solutions in [5]. The primary steps of designing an RDH scheme approaching the rate-distortion bound can be described as shown in Fig. 3.

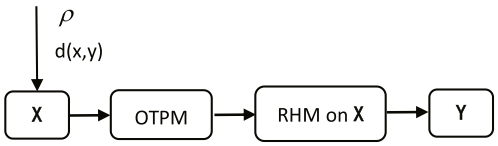

Fig. 3. Primary steps of designing an RHM scheme.

3. Proposed schemes

3.1. Algorithm overview

For RDH, RHM is a theoretically and experimentally proven modification method that is expected to be applied for optimizing the modification of grayscale-invariance RDH. To achieve this, we must establish the rate-distortion model of grayscale-invariance RDH and solve it. Before establishing the rate-distortion model, we first describe our framework by introducing RHM.

For grayscale-invariance RDH, we must select green scales for adaptive adjustment to keep grayscale invariance because only the weight of the green scale is greater than 0.5, yielding a one-bit error correction message for recovery. The tasks of red scales and blue scales for accommodating secret messages and error correction messages can be exchanged. For convenience, following Hou et al.'s work [33], we select red scales to accommodate secret messages and blue scales to accommodate error correction messages; then, green scales are adaptively adjusted to maintain grayscale invariance. However, instead of the pixel-by-pixel embedding method, in our framework, the host color pixels are divided into p disjoint subsequences according to RHM, and the messages are embedded subsequence by subsequence.

The overview of the proposed operations is described as Fig. 4. Given the payload, we first embed all of the secret messages into red scales subsequence by subsequence through RHM. After finishing modification on red scales, we start error correction messages embedding by modifying blue scales subsequence by subsequence. In detail, for $\mathbf{r}_i$, $\mathbf{g}_i$ and $\mathbf{b}_i$, $1 \leq i \leq p$, we locate the indices of modified red scales in $\mathbf{r}_i$ and collect the blue scales in $\mathbf{b}_i$ at the modified indices. The error correction messages from $\mathbf{g}_{i-1}$ denoted as $\mathbf{EC_{i-1}}$ will be embedded into the collected blue scales. To maintain grayscale invariance, the green scales at the modified indices of $\mathbf{g}_i$

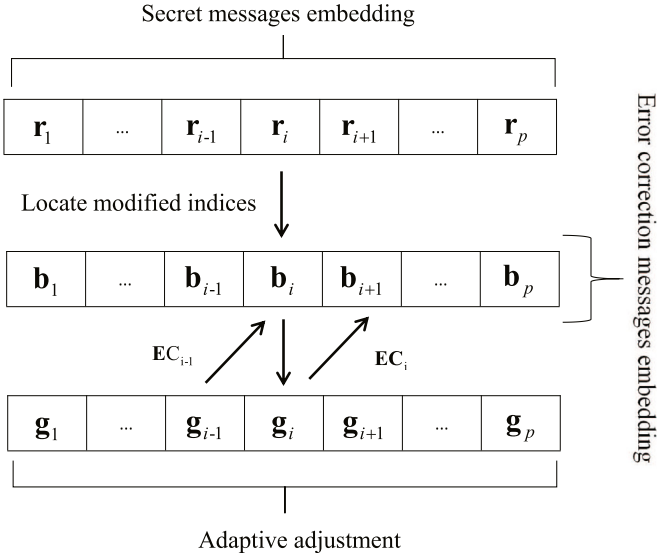

Fig. 4. Overview of the proposed operations.

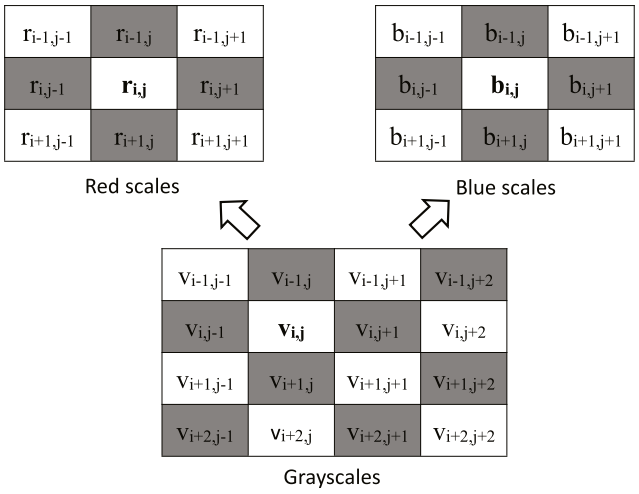

Fig. 5. Checkerboard pattern.

Fig. 6. Tested color images of size 510 × 510.

will be adaptively adjusted. Of course, at the same time, $\mathbf{EC_i}$ will be obtained from the modified indices of $\mathbf{g}_i$ for the next $\mathbf{b_{i+1}}$ to accommodate.

As seen in the above framework, the modified indices and magnitudes of green scales and blue scales are determined on the modifications of red scales. To minimize the total modification distortion, the number of red scales should be modified, and the method for the optimal modification of red scales is the key to the successful implementation of the algorithm.

3.2. Linear predictor based on separable grayscales

As shown in Eq. (1), for RDH, a smaller entropy of the host sequence, i.e., a sharper host histogram, leads to better RDH performance. Similar to most RDH algorithms, the PEs of image pixels are the most commonly used host sequence. Invariant grayscales are strongly correlated with each color channel so that a sharper host histogram can be generated by exploring such correlations. The pixels of the host image are divided into two parts, as seen in Fig. 5, and the messages are embedded part by part. If white pixels are used to carry messages, dark pixels will not be modified and vice versa.

Based on invariant grayscales, Hou et al. utilize a 2nd-order polynomial to predict the red and blue scales. Taking the prediction of red scale $r_{i,j}$ as an example, its prediction value $\hat{r}_{i,j}$ is

$$\hat{r}_{i,j} = a + bv_{i,j} + cv_{i,j}^2, \tag{7}$$

where the polynomial coefficients are optimized by minimizing the fitting errors with $\{v_{i+1,j}, v_{i-1,j}, v_{i,j+1}, v_{i,j-1}\}$ as inputs and $\{r_{i+1,j}, r_{i-1,j}, r_{i,j+1}, r_{i,j-1}\}$ as outputs.

However, we find that there is no need to use a 2nd-order polynomial, and a linear polynomial is sufficient. The reason is that the squared scales are usually very large and a small fluctuation in c will result in a large deviation so that for a 2nd-order polynomial, the calculated coefficient c is usually close to 0. Based on the above observations, we adopt a linear predictor to reduce the computational complexity as given by

$$f_l(v_{i,j}) = a + bv_{i,j}. \tag{8}$$

Of course, the coefficients $\{a, b\}$ are determined by the least squares method, similar to Hou et al.'s method.

From Eq. (2) we get that grayscales are the weighted combinations of red, green and blue scales, which can be applied to predict red scales and blue scales. To predict the red scale $r_{i,j}$, grayscales $\{v_{i+1,j}, v_{i-1,j}, v_{i,j+1}, v_{i,j-1}\}$ are inputs and $\{r_{i+1,j}, r_{i-1,j}, r_{i,j+1}, r_{i,j-1}\}$ are outputs. After obtaining the optimal polynomial coefficients $\{a, b\}$, we obtain $\hat{r}_{i,j} = f_l(v_{i,j})$.

At the receivers side, we first restore red scales. After red scales are determined, the correlations between grayscales and blue scales can be further improved. Before predicting blue scales, we eliminate the effects of red scales from grayscales as

$$v_{i,j}^s = \lfloor (v_{i,j} - 0.299 r_{i,j})/(1 - 0.299) \rceil, \tag{9}$$

where $v_{i,j}^s$ is called separable grayscale. For the prediction of the blue scale $b_{i,j}$, different from the strategy [33], we use the separable grayscales $\{v_{i+1,j}^s, v_{i-1,j}^s, v_{i,j+1}^s, v_{i,j-1}^s\}$ and $\{b_{i+1,j}, b_{i-1,j}, b_{i,j+1}, b_{i,j-1}\}$ as references. It is clear that the correlations between separable grayscales and blue scales are stronger. After obtaining the optimal polynomial coefficients, we obtain the prediction scale $\hat{b}_{i,j}$ as $\hat{b}_{i,j} = f_l(v_{i,j}^s)$.

By subtracting $\{\hat{r}_{i,j}, \hat{b}_{i,j}\}$ from the original scales $\{r_{i,j}, b_{i,j}\}$, we obtain their PEs $\{e_{i,j}^r, e_{i,j}^b\}$ as

$$\begin{cases} e_{i,j}^r = r_{i,j} - \hat{r}_{i,j}, \\ e_{i,j}^b = b_{i,j} - \hat{b}_{i,j}. \end{cases} \tag{10}$$

To demonstrate the advantages of the linear predictor based on separable grayscales, we compare it with Hou et al.'s 2nd-order polynomial predictor and the average filter predictor. The average PEs from airplane, Barbara, Lena, baboon are shown in Fig. 7.

As mentioned above, it is not necessary to use a 2nd-order polynomial, and a linear polynomial is sufficient. The distribution of red scales' PEs from the linear polynomial will be even slightly better than that of the 2nd-order polynomial, as illustrated in Fig. 7(a), while the computational complexity is reduced. Because we eliminate the effects of red scales and obtain a better reference, i.e., separable grayscale, the distribution of the blue scale PEs is much sharper than that from Hou et al.'s predictor, as seen in Fig. 7(b).

After obtaining PEs, we embed the message by modifying $\{e_{i,j}^r, e_{i,j}^b\}$ to $\{e_{i,j}'^r, e_{i,j}'^b\}$, and then, the marked scales will be obtained according to

$$\begin{cases} r_{i,j}' = \hat{r}_{i,j} + e_{i,j}'^r \\ b_{i,j}' = \hat{b}_{i,j} + e_{i,j}'^b \end{cases}. \tag{11}$$

At the receiver's end, we first calculate the marked PEs of the red scales based on the invariant grayscales from which we restore red scales and secret messages. Next, we eliminate the effects of red scales and obtain separable grayscales, based on which we calculate the marked PEs of the blue scales, and further restore the

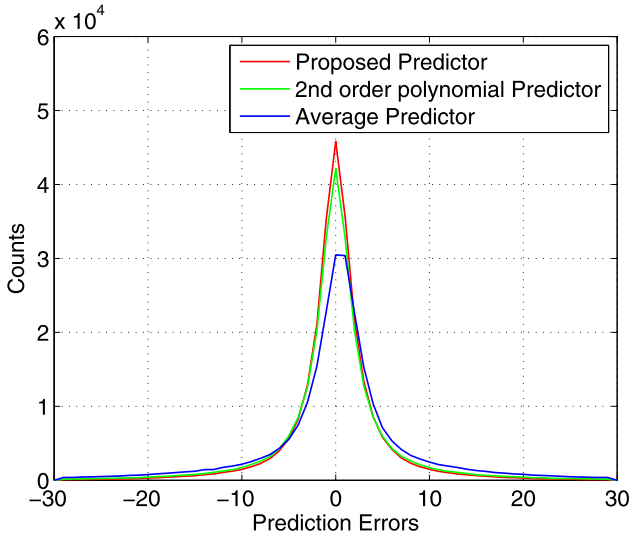

(a) Average PEs from red scales

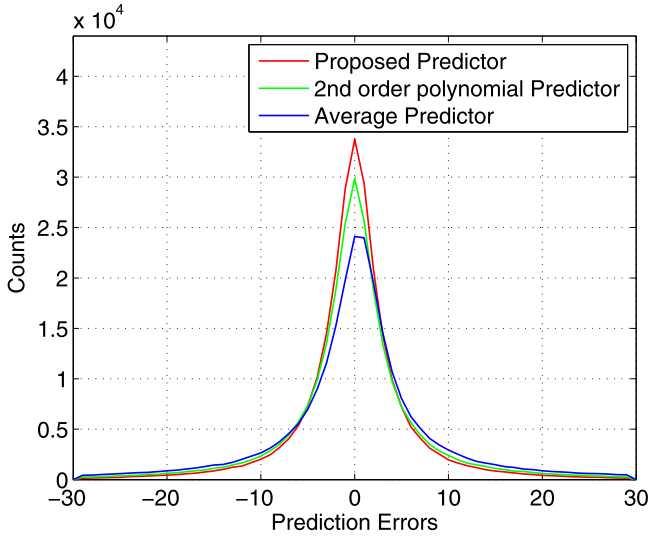

(b) Average PEs from blue scales

Fig. 7. PE distributions of three predictors.

blue scales and error correction messages. Finally, green scales will be also restored according to error correction messages.

3.3. Rate-distortion bound of grayscale-invariance RDH

3.3.1. Rate-distortion bound for general distortion metric

As shown in Fig. 4, red scales are utilized to accommodate secret messages. For N selected host pixels (r_i, g_i, b_i), $1 \le i \le N$, we first collect the PEs of the host red scales as $\mathbf{X}_R = (Er_1, \cdots, Er_N)$, which can be obtained by subtracting the prediction values from the original scales. Once the embedding rate ρ is given, based on the defined distortion metric for red scales and the probability distribution of $\mathbf{X}_R$ denoted as $P_{X_R}(x)$, the OTPM $P_{Y_R|X_R}(y|x)$ can be well estimated. According to $P_{Y_R|X_R}(y|x)$, $\mathbf{X}_R$ is modified to $\mathbf{Y}_R = (Er'_1, \cdots, Er'_N)$, correspondingly $\mathbf{R} = (r_1, \cdots, r_N)$ is modified to $\mathbf{R}' = (r'_1, \cdots, r'_N)$.

Next, we determine the modified indices as $\mathbf{MI} = (id_1, \cdots, id_K)$, for which $r_{id_j} \ne r'_{id_j}$, $1 \le j \le K$. According to $\mathbf{MI}$, we extract green scales as $\mathbf{G}_M = (g_{id_1}, \cdots, g_{id_K})$, and blue scales as $\mathbf{B}_M = (b_{id_1}, \cdots, b_{id_K})$, to be modified. The error correction messages are embedded by modifying $\mathbf{B}_M$ to $\mathbf{B}'_M = (b'_{id_1}, \cdots, b'_{id_K})$; then, $\mathbf{G}_M$ will be adaptively adjusted to $\mathbf{G}'_M = (g'_{id_1}, \cdots, g'_{id_K})$ to keep grayscales $\mathbf{V}_M = (v_{id_1}, \cdots, v_{id_K})$ unchanged.

After the modification is carried out, the distortion only occurs in the located modified indices so that the average distortion for the N host pixels denoted by J_{ave} is

$$\begin{aligned} J_{ave} &= \frac{1}{N}\sum_{i=0}^{N}(d(r_i, r'_i) + d(g_i, g'_i) + d(b_i, b'_i)) \\ &= \frac{1}{N}\left(\sum_{i=0}^{N} d(r_i, r'_i) + \sum_{j=0}^{K}(d(g_{id_i}, g'_{id_i}) + d(b_{id_i}, b'_{id_i}))\right) \\ &= \frac{1}{N}\sum_{i=0}^{N}(d(r_i, r'_i) + f_s(|r'_i - r_i|)(d(g_i, g'_i) + d(b_i, b'_i))), \end{aligned} \tag{12}$$

where

$$f_s(a) = \begin{cases} 0, & \text{if } a = 0, \\ 1, & \text{if } a > 0. \end{cases} \tag{13}$$

The modifications on such three color scales are interrelated, and Eq. (12) shows the joint distortion. The optimization of the interrelated modification manner such that this joint distortion is minimized gives a modification-dependent model. The existing RCC schemes can be only applied to solve modification-independent optimization, where the modifications of different elements are independent. In the following, we will decompose joint modification and associate the modification distortions of green and blue scales with those of the red scales so that the modification-dependent distortion can be appropriately formulated as a modification-independent distortion.

Since each modified index will yield a one-bit error correction message, the volume of the error correction messages is the same as the volume of the determined blue scales, i.e., equal to the volume of the modified red scales. Assuming the PEs' probability distribution of $\mathbf{B} = (b_1, \cdots, b_N)$ is $P_{X_B}(x)$, we will execute RHM on PEs by the embedding rate $\rho = 1$. Of course, there may exist some cases that host blue sequence cannot provide enough embedding rate. In such cases, we just need to reduce the embedding rate, and reserve more invariant pixels to accommodate the extra error correction messages. Once embedding rate and $P_{X_B}(x)$ are determined, the OTPM $P_{Y_B|X_B}(y|x)$ can be calculated, based on which the average distortion for the blue scales denoted as $J_{B_{ave}}$ will be also determined such that

$$J_{B_{ave}} = \sum_{x=0}^{m-1}\sum_{y=0}^{n-1} P_{X_B}(x) P_{Y_B|X_B}(y|x) d(x, y). \tag{14}$$

According to the indices of modified red scales, we sample the sequence $\mathbf{B}_M = (b_{id_1}, \cdots, b_{id_K})$ from $\mathbf{B} = (b_1, \cdots, b_N)$. $\mathbf{B}_M$ and $\mathbf{B}$ come from the same distribution, thus their PEs tend to share the same probability distribution $P_{X_B}(x)$. Once the current red scale is modified, regardless of its modification amplitude, the summed distortion will be proportional to the volume of $\mathbf{B}_M$, i.e., K, so that

$$\sum_{i=0}^{N} f_s(|r'_i - r_i|) d(b_i, b'_i) = \sum_{j=0}^{K} d(b_{id_j}, b'_{id_j}) = K J_{B_{ave}}. \tag{15}$$

Therefore, we associate the modification distortion of blue scales with that of the red scales. Such distortion is not related to the red scales' modification amplitudes and instead depends only on the number of their modified indices, i.e., K. For different distortion metrics and host sequences, $J_{B_{ave}}$ may be different, but it can be exactly calculated according to $P_{X_B}(x)$ and the given distortion metric.

For each green scale, its modification is determined by the modifications of the red scale and the blue scale at the same index. Because secret messages are embedded into red scales, to establish the rate-distortion model for grayscale-invariance RDH and solve it, we must decompose the joint modification and associate the modification distortions of green scales with those of the red scales. Assume that the association can be formulated by a mapping function with r_i and r'_i as the variables, that is,

$$d(g_i, g'_i) = f_s(|r'_i - r_i|) f_g^m(r_i, r'_i). \tag{16}$$

For different distortion metrics, the mapping functions may have different forms. In the next section, we will specify the appropriated mapping function f_g^m in terms of the square error distortion metric. After finding such a mapping function, we obtain

$$\sum_{j=0}^{K} d(g_{id_j}, g'_{id_j}) = \sum_{i=0}^{N} f_s(|r'_i - r_i|) f_g^m(r_i, r'_i). \tag{17}$$

According to the RCC scheme, OTPM $P_{Y_R|X_R}(y|x)$ implies the modification manner, according to which we modify $\mathbf{X}_R$ to $\mathbf{Y}_R$, i.e., $\mathbf{R}$ to $\mathbf{R}'$, and the modified indices can be also observed by the OTPM. Based on Eqs. (15) and (17) and through the substitution of variables, Eq. (12) can be reformulated as

$$J_{ave} = \sum_{x=0}^{m-1} \sum_{y=0}^{n-1} P_{X_R}(x) P_{Y_R|X_R}(y|x) (d(x, y) + f_s(|y - x|)(J_{B_{ave}} + f_g^m(x, y))), \tag{18}$$

where x, y are in the sets of host red scales and marked red scales respectively.

Secret messages are embedded into red scales, and the embedding rate ρ satisfies

$$H(\mathbf{Y}_R) = \rho + H(\mathbf{X}_R). \tag{19}$$

Based on the above discussion, the rate-distortion bound of grayscale-invariance RDH can be formulated as

Model I

$$\begin{aligned} \text{Min} \quad & \sum_{x=0}^{m-1} \sum_{y=0}^{n-1} P_{X_R}(x) P_{Y_R|X_R}(y|x) d_{jt}(x, y), \\ \text{s.t.} \quad & H(\mathbf{Y}_R) = \rho + H(\mathbf{X}_R) \end{aligned} \tag{20}$$

where the joint distortion metric for red scales is given by

$$d_{jt}(x, y) = d(x, y) + f_s(|y - x|)(J_{B_{ave}} + f_g^m(x, y)). \tag{21}$$

If we can successfully establish the relationship between the modification distortions of the green scales with that of the red scales, the modification-dependent optimization becomes a problem of how to optimize the modification of red scales in order to minimize the total distortion, i.e., Model I. Model I is a modification-independent model that can be solved by the existing RCC schemes.

3.3.2. Rate-distortion bound for square error distortion metric

For different distortion metrics, the average distortion $J_{B_{ave}}$ occurring from blue scales can be calculated exactly, while that from green scales may vary. For RDH, the most commonly used metric is the squared error distortion metric, i.e., $d(x, y) = (x - y)^2$. Taking $d(x, y) = (x - y)^2$ as an example, we elaborate on how to appropriate the mapping from the green scales' modification distortion to the red scales' modification distortion.

After modifying $\{r_{id_j}, b_{id_j}\}$ to $\{r'_{id_j}, b'_{id_j}\}$, g_{id_j} must be adjusted to g'_{id_j} to maintain the grayscale invariance according to

$$g'_{id_j} = f_{v2g}(r'_{id_j}, b'_{id_j}, v_{id_j}). \tag{22}$$

Therefore,

$$d(g_{id_j}, g'_{id_j}) = d(g_{id_j}, f_{v2g}(r'_{id_j}, b'_{id_j}, v_{id_j})). \tag{23}$$

Assuming $\Delta r_{id_j} = r'_{id_j} - r_{id_j}$ and $\Delta b_{id_j} = b'_{id_j} - b_{id_j}$, according to Eq. (22), we have

$$\begin{aligned} |\Delta g_{id_j}| &= |g'_{id_j} - g_{id_j}| \\ &= |(v_{id_j} - 0.299 r'_{id_j} - 0.114 b'_{id_j})/0.587 \\ &\quad - (v_{id_j} - 0.299 r_{id_j} - 0.114 b_{id_j})/0.587| \\ &= |(0.299 \Delta r_{id_j} + 0.114 \Delta b_{id_j})/0.587| \\ &= |(0.51 \Delta r_{id_j} + 0.19 \Delta b_{id_j})|. \end{aligned} \tag{24}$$

For green scales, their total distortion is

$$\sum_{j=0}^{K} |\Delta g_{id_j}|^2 = \sum_{j=0}^{K} (0.26 \Delta r_{id_j}^2 + 0.036 \Delta b_{id_j}^2 + 0.194 \Delta r_{id_j} \Delta b_{id_j}). \tag{25}$$

Since the distributions of Δr_{id_j} and Δb_{id_j} are randomly centered at 0,

$$\sum_{j=0}^{K} \Delta r_{id_j} \Delta b_{id_j} = 0. \tag{26}$$

Combined with

$$\sum_{j=0}^{K} \Delta b_{id_j}^2 = K J_{B_{ave}}, \tag{27}$$

we obtain

$$\sum_{j=0}^{K} |\Delta g_{id_j}|^2 = 0.26 \sum_{i=0}^{N} f_s(|r'_i - r_i|)(r'_i - r_i)^2 + 0.036 K J_{B_{ave}}. \tag{28}$$

That is, the mapping function Eq. (16) is given by

$$d(g_i, g'_i) = f_s(|r'_i - r_i|)(0.26(r'_i - r_i)^2 + 0.036 J_{B_{ave}}). \tag{29}$$

Now, we associate the modifications of the green scales with that of the red scales. Compared to the total distortion, $0.036 J_{B_{ave}}$ can be neglected; thus, the joint distortion metric for red scales becomes

$$d_{jt}(x, y) = 1.26(x - y)^2 + f_s(|y - x|) J_{B_{ave}}. \tag{30}$$

Based on the above discussion, Model I can be reformulated for the squared error distortion metric as

Model II

$$\begin{aligned} \text{Min} \quad & \sum_{x=0}^{m-1} \sum_{y=0}^{n-1} P_{X_R}(x) P_{Y_R|X_R}(y|x) (1.26(x - y)^2 + f_s(|y - x|) J_{B_{ave}}). \\ \text{s.t.} \quad & H(\mathbf{Y}_R) = \rho + H(\mathbf{X}_R) \end{aligned} \tag{31}$$

3.4. Recursive embedding and extracting algorithms

To extract the embedded messages and restore the host image losslessly, the receiver needs some auxiliary parameters, including the probability distribution of the red scales' PEs $P_{X_R}(x)$, the probability distribution of the blue scales' PEs $P_{X_B}(x)$, $J_{B_{ave}}$, the embedding rate ρ, and the residuals of the overflow/underflow pixels. Similar to that with most RDH algorithms, we reserve some invariant pixels for recording these parameters, where the invariant pixel means that Eq. (32) holds for the current pixel $\{r, g, b\}$.

$$f_{c2v}(r, g, 2\lfloor \frac{b}{2} \rfloor) = f_{c2v}(r, g, 2\lfloor \frac{b}{2} \rfloor + 1) \tag{32}$$

These auxiliary parameters will be embedded into the least significant bits (LSBs) of blue scales of reserved invariant pixels, and

these substituted LSBs will be regarded as a part of the secret messages to be embedded.

Based on the above discussion, we elaborate on the embedding and extracting algorithms as follows.

Recursive embedding algorithm

1. Reserve some invariant pixels and add LSBs of the blue scales from reserved pixels to the secret messages.
2. Based on grayscales and red scales, calculate separable grayscales and further obtain blue scales' PEs; based on grayscales, obtain red scales' PEs.
3. According to $P_{X_B}(x)$ and $d(x, y)$, calculate the OTPM_B for blue scales and subsequently obtain $J_{B_{ave}}$.
4. Define joint distortion metric $d_{jt}(x, y)$ for red scales according to Eq. (21); combined with $P_{X_R}(x)$ and the embedding rate ρ, obtain OTPM_R.
5. Divide the host pixels into p subsequences and obtain the subsequences $\mathbf{r}_i$, $\mathbf{g}_i$ and $\mathbf{b}_i$, for $i = 1, 2, ..., p$.
6. Finish embedding secret messages into red scales' PEs subsequence by subsequence according to OTPM_R through RHM.
7. For each subsequence, locate the modified indices in $\mathbf{r}_i$ and collect the blue scales in $\mathbf{b}_i$ at the modified indices. According to OTPM_B, embed $\mathbf{EC_{i-1}}$ from $\mathbf{g}_{i-1}$ into the collected blue scales' PEs with RHM.
8. Green scales in $\mathbf{g}_i$ at the modified indices will be adaptively adjusted, and at the same time $\mathbf{EC_i}$, will yield from the modified indices for the next $\mathbf{b_{i+1}}$ to accommodate.
9. Embed the auxiliary information into the LSBs of reserved blue scales.

Recursive extracting algorithm

1. Extract auxiliary information from the reserved blue scales.
2. Based on the invariant grayscales, obtain the marked PEs of red scales.
3. Define $d_{jt}(x, y)$, combined with $P_{X_R}(x)$ and ρ, obtain OTPM_R.
4. Divide the marked pixels into p subsequence and decode secret messages from marked red scales' PEs subsequence by subsequence according to OTPM_R.
5. Based on grayscales and restored red scales, calculate separable grayscales and further obtain the marked PEs of blue scales.
6. For each subsequence, determine the modified indices in $\mathbf{r}_i$ and collect the blue scales in $\mathbf{b}_i$ at the modified indices. According to OTPM_B, decode $\mathbf{EC_{i-1}}$ from the collected marked blue scales' PEs.
7. Readjust green scales at the modified indices of $\mathbf{g}_i$ according to the restored red scales and blue scales and the $\mathbf{EC_i}$.
8. Reconstruct the reserved blue scales using the extracted LSBs.

4. Experimental results

4.1. Validity of the proposed model

The proposed model is an extended RCC scheme applied for grayscale-invariance RDH, and its key is to establish the association of modification distortions of the green scales and the blue scales with that of the red scales. By associating the modification distortions of their color scales, we define the joint distortion metric for red scales. Taking the square error distortion metric as an example, to confirm the validity of the joint distortion metric $d_{jt} = 1.26(x-y)^2 + f_s(|y-x|)J_{B_{ave}}$, we compare it with four different distortion metrics, including

$$\begin{cases} d_1(x,y) = (x-y)^2 \\ d_2(x,y) = 1.26(x-y)^2 \\ d_3(x,y) = 0.26(x-y)^2 + f_s(|y-x|)J_{B_{ave}} \\ d_4(x,y) = (x-y)^2 + f_s(|y-x|)J_{B_{ave}} \end{cases}. \tag{33}$$

The rate-distortion performances under different distortion metrics and payloads are plotted in Fig. 8, where the assessment indicator is PSNR. To show the joint modification more clearly, we describe the distortion distribution separately for the red, green and blue scales. As seen in Table 1, the percentile data are given by

$$\left\{ \frac{J_{R_{ave}}}{J_{R_{ave}} + J_{G_{ave}} + J_{B_{ave}}}, \frac{J_{G_{ave}}}{J_{R_{ave}} + J_{G_{ave}} + J_{B_{ave}}}, \frac{J_{B_{ave}}}{J_{R_{ave}} + J_{G_{ave}} + J_{B_{ave}}} \right\}, \tag{34}$$

where $J_{R_{ave}}$, $J_{G_{ave}}$, $J_{B_{ave}}$ are the average distortions from the red, green, and blue scales, respectively.

As observed in Fig. 8, except for House, RHM with $d_1(x, y) = (x-y)^2$ will perform poorly, proving that the current RCC schemes usually cannot be applied directly for grayscale-invariance RDH. However, by extending RHM with $d_{jt}(x, y) = 1.26(x-y)^2 + f_s(|y-x|)J_{B_{ave}}$, its performance can be significantly improved.

If we neglect the modification distortion of blue scales and define $d_2(x, y) = 1.26(x-y)^2$, the performance will be nearly the same as $d_1(x, y) = (x-y)^2$ because they belong to the same distortion metric without considering the blue scales' modification. Metrics not considering blue scales' modification will usually cause few distortions for the red and green scales but will introduce a very large distortion for the blue scales, as seen in Table 1 for $d_1(x, y)$ and $d_2(x, y)$. By the same token, metric $d_3(x, y)$ barely considering red scales' modification distortion will usually cause large distortion for red scales, as seen in Table 1 for $d_3(x, y)$.

On the other hand, if we neglect the modification distortion of the green scales and define $d_4(x, y) = (x-y)^2 + J_{B_{ave}}$, its performance will be just slightly less than $d_{jt}(x, y)$. The reason is that the distortion arising from the green scales accounts for a small part of the total distortion, as seen in Table 1 for $d_{jt}(x, y)$ and $d_4(x, y)$.

Note that, as for House, the performances under $d_1(x, y)$, $d_2(x, y)$, $d_4(x, y)$ and $d_{jt}(x, y)$ are similar, because the PE histogram form blue scales of House is very sharp so that the corresponding $J_{B_{ave}}$ is as small as 0.5 and is nearly negligible. Therefore, the metrics $d_1(x, y)$, $d_2(x, y)$, $d_4(x, y)$ and $d_{jt}(x, y)$ show nearly the same performance.

Through RHM under $d_{jt}(x, y)$, the modification can be adaptively optimized, thus achieving the best rate-distortion performance. Now, we proved the validity of the proposed rate-distortion model for grayscale-invariance RDH in experiments.

4.2. Rate-distortion performance

In this subsection, we compared the proposed method with Hou et al.'s method [33] and Gaoet al.'s method [34]. The schemes in [33,34] embed messages by difference expansion without reasonable distortion-control strategy. By finding the optimal modification minimizing the total distortion theoretically, we achieve encouraging rate-distortion performances for all of the test images listed in Fig. 6.

As shown in Fig. 9, the rate-distortion performances can be significantly improved compared to Hou et al..'s method [33] and Gao et al.'s method [34]. Of course, all the above methods will keep the graysales unchanged and thus do not disturb the marked images' further applications in many cases. Our advantages own to two aspects: The first one is that we utilize separable grayscales as the references to predict the blue scales, therefore, yielding much sharper host histogram as seen in Fig 7. For RDH, the sharper the host histogram is, the better the performance of RDH. The second reason is that we find the optimal modification theoretically minimizing the total distortion for grayscale-invariance RDH, while the existing methods can not.

We also show the time complexities for the above three algorithms implemented in MATLAB 2014, and the test machine is a Lenovo personal computer with an i3-4130 CPU @ 3.40 GHz and 4.00 GB of RAM. Taking embedding 10, 000 bits as examples,

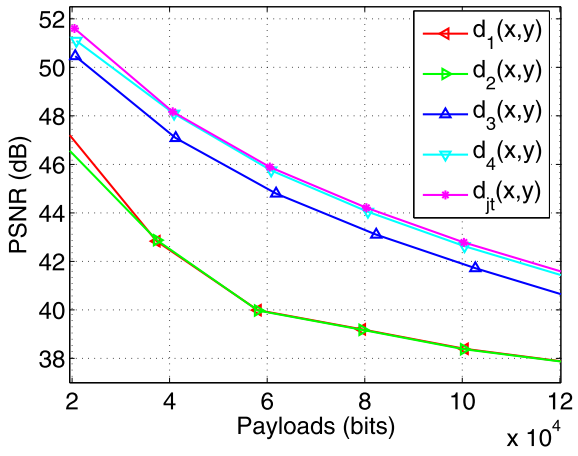

(a) Lena

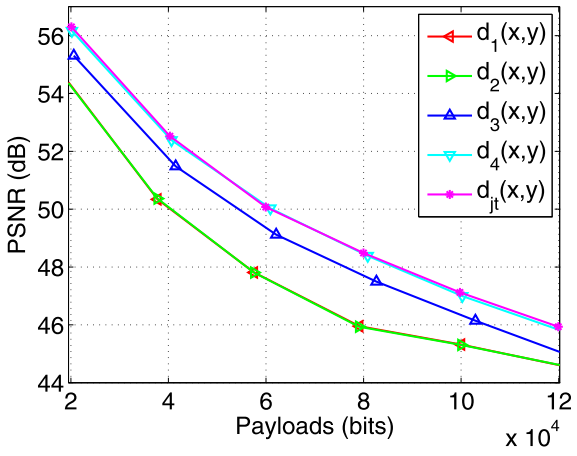

(b) Barbara

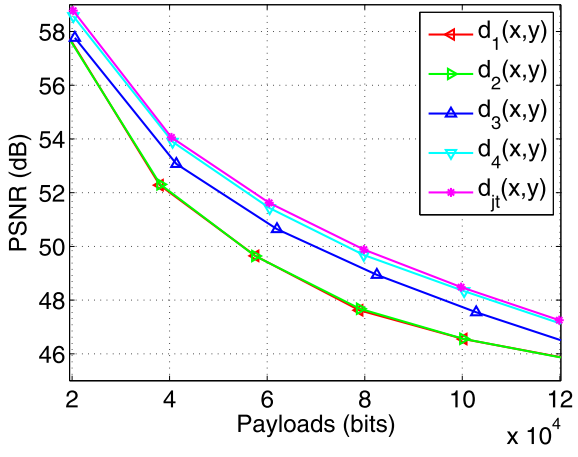

(c) Airplane

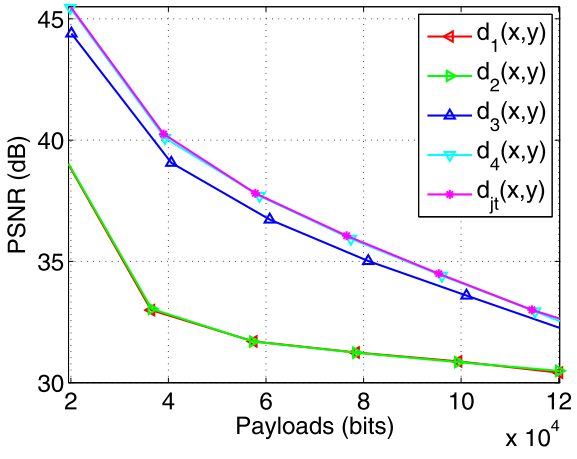

(d) Baboon

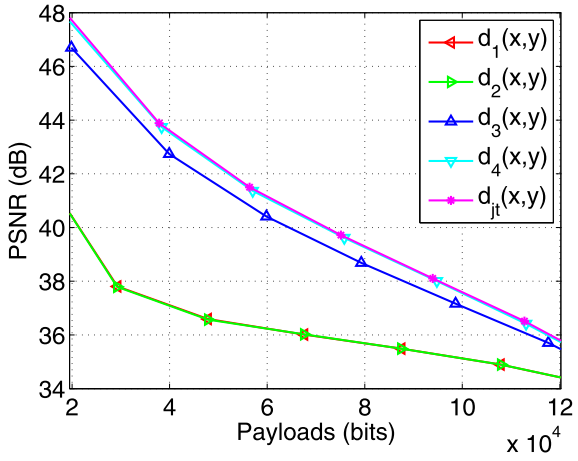

(e) Pepper

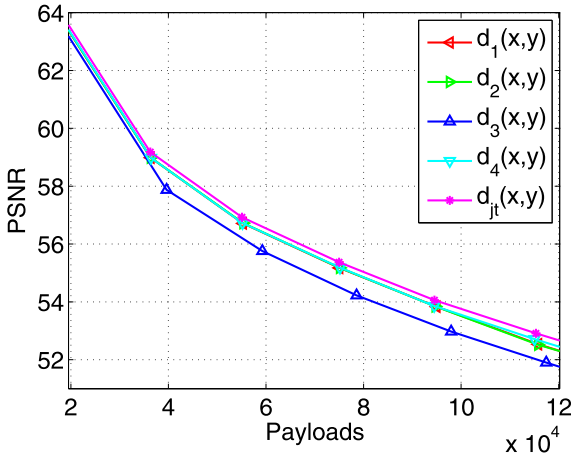

(f) House

Fig. 8. Rate-distortion performances under different distortion metrics.

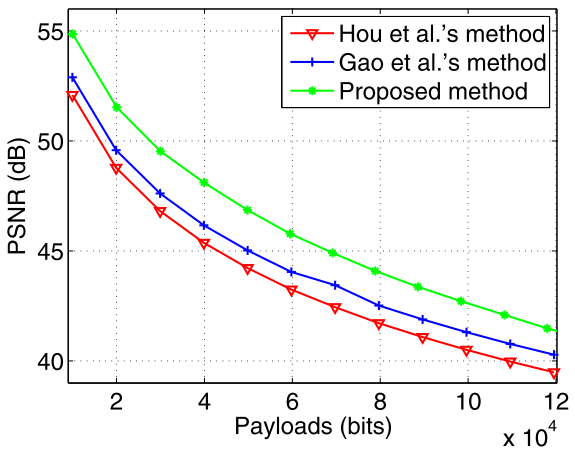

(a) Lena

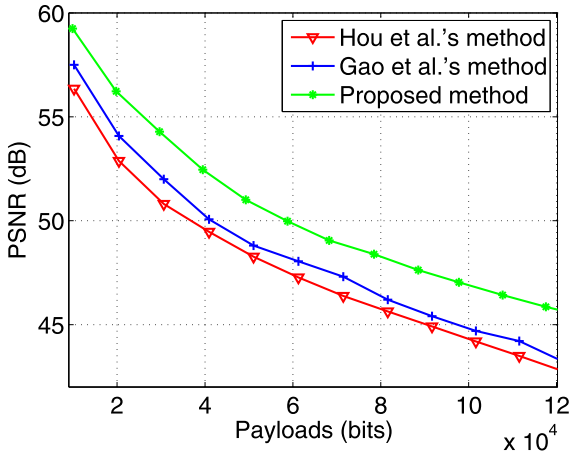

(b) Barbara

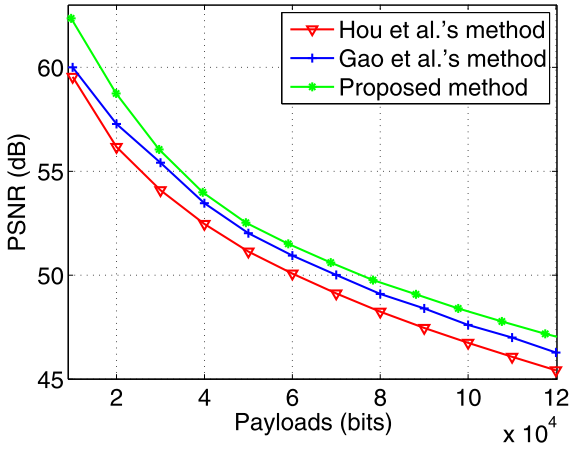

(c) Airplane

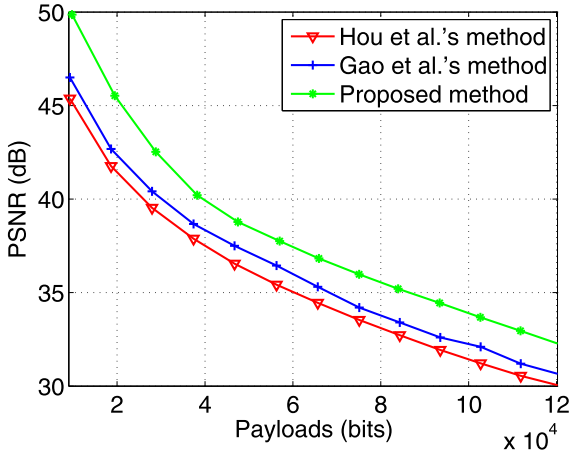

(d) Baboon

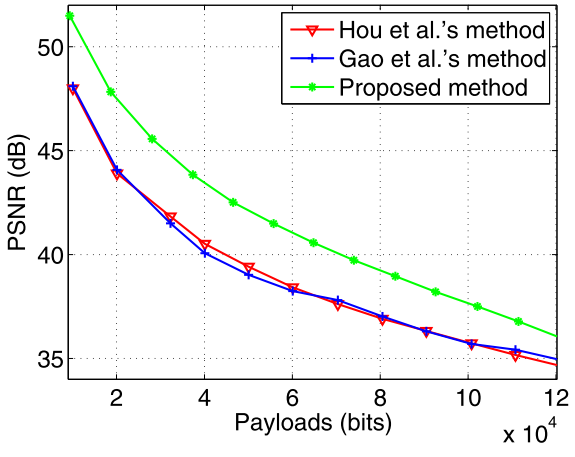

(e) Pepper

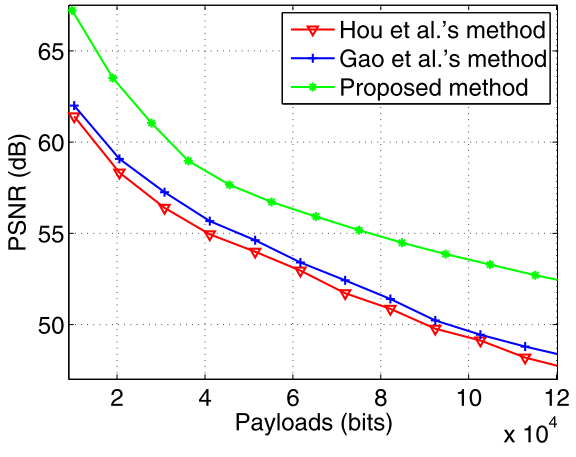

(f) House

Fig. 9. Rate-distortion performances of Hou et al.'s method and the proposed method.

Table 1
Distortion distributions for red, green and blue scales.

Payloads (bits)		40000	80000	120000
Lena	d_1	{3%, 5%, 92%}	{5%, 5%, 90%}	{10%, 6%, 84%}
	d_2	{3%, 5%, 92%}	{5%, 5%, 90%}	{10%, 6%, 84%}
	d_3	{62%, 17%, 21%}	{63%, 17%, 20%}	{63%, 17%, 20%}
	d_4	{43%, 12%, 45%}	{41%, 12%, 47%}	{42%, 13%, 45%}
	d_{jt}	{40%, 12%, 48%}	{37%, 11%, 52%}	{37%, 11%, 52%}
Barbara	d_1	{10%, 10%, 80%}	{10%, 10%, 80%}	{20%, 12%, 68%}
	d_2	{10%, 10%, 80%}	{10%, 10%, 80%}	{20%, 12%, 68%}
	d_3	{63%, 19%, 18%}	{63%, 19%, 18%}	{63%, 19%, 18%}
	d_4	{40%, 16%, 41%}	{43%, 16%, 41%}	{44%, 16%, 40%}
	d_{jt}	{33%, 15%, 52%}	{37%, 15%, 49%}	{38%, 15%, 48%}
Airplane	d_1	{13%, 12%, 75%}	{12%, 11%, 77%}	{20%, 12%, 68%}
	d_2	{13%, 12%, 75%}	{12%, 11%, 77%}	{20%, 12%, 68%}
	d_3	{61%, 20%, 19%}	{62%, 19%, 19%}	{62%, 19%, 19%}
	d_4	{39%, 17%, 44%}	{35%, 15%, 50%}	{42%, 16%, 42%}
	d_{jt}	{36%, 16%, 48%}	{35%, 15%, 50%}	{36%, 15%, 49%}
Baboon	d_1	{2%, 4%, 95%}	{5%, 5%, 90%}	{14%, 6%, 80%}
	d_2	{2%, 4%, 95%}	{5%, 5%, 90%}	{14%, 7%, 79%}
	d_3	{41%, 17%, 18%}	{65%, 17%, 18%}	{65%, 17%, 18%}
	d_4	{42%, 12%, 46%}	{42%, 12%, 46%}	{43%, 13%, 44%}
	d_{jt}	{37%, 11%, 52%}	{38%, 11%, 51%}	{40%, 12%, 48%}
Pepper	d_1	{3%, 5%, 93%}	{9%, 6%, 85%}	{23%, 9%, 69%}
	d_2	{3%, 5%, 92%}	{9%, 6%, 85%}	{23%, 9%, 69%}
	d_3	{64%, 17%, 19%}	{65%, 17%, 18%}	{65%, 17%, 18%}
	d_4	{42%, 13%, 44%}	{42%, 13%, 45%}	{46%, 13%, 41%}
	d_{jt}	{36%, 11%, 52%}	{39%, 12%, 49%}	{43%, 13%, 44%}
House	d_1	{36%, 27%, 37%}	{35%, 25%, 40%}	{35%, 25%, 40%}
	d_2	{36%, 27%, 37%}	{35%, 25%, 40%}	{35%, 25%, 40%}
	d_3	{60%, 26%, 14%}	{58%, 26%, 16%}	{60%, 25%, 15%}
	d_4	{36%, 27%, 37%}	{35%, 25%, 40%}	{40%, 25%, 35%}
	d_{jt}	{36%, 27%, 37%}	{34%, 26%, 40%}	{39%, 25%, 36%}

Table 2
Speed comparisons of three algorithms.

Image	Lena	Barbara	Airplane	Baboon	Pepper	House
Hou et al. [33]	66	60	66	170	122	64
Gao et al. [34]	108	130	84	420	365	120
Proposed method	70	70	71	72	68	65

the embedding times (measured in seconds) of three algorithms are listed in Table 2. From this Table we observe that the time complexities of Hou et al.'s method [33] and Gao et al.'s method [34] for images with rich texture, such as Baboon, will be much higher due to their pixel selection strategies. However, by the proposed method, the time complexities are relatively stable for the test images.

5. Conclusion

By converting the modification-dependent model to the modification-independent model, we successfully applied the theoretically proven optimal RHM in grayscale-invariance RDH and achieved encouraging results. Our method is advantageous for two reasons. First, we propose a linear predictor based on separable grayscales to yield a sharper host histogram, and more importantly, we establish a rate-distortion model for grayscale-invariance RDH in order to find the optimal joint modification method and minimize the total distortion theoretically.

For different distortion metrics, the distortion mapping from the green scales to red scales may be different. In this paper, we only provide the appropriated mapping for the squared error distortion metric. Determining how to establish the distortion mapping for general distortion metrics is still a challenging problem.

Declaration of Competing Interest

The authors declare that they have no known competing financial interests or personal relationships that could have appeared to influence the work reported in this paper.

CRediT authorship contribution statement

Siyan Zhou: Methodology, Software, Investigation. **Weiming Zhang:** Validation, Formal analysis, Data curation. **Chaomin Shen:** Resources, Writing - review & editing, Supervision.

Acknowledgements

This work was supported by the National Natural Science Foundation of China under Grants 61572452, U1636201, 61731009, 11771276, and in part by the Science and Technology Commission of Shanghai Municipality under Grant 14DZ2260800.

Supplementary material

Supplementary material associated with this article can be found, in the online version, at doi:10.1016/j.sigpro.2020.107562.

References

[1] A.S. Brar, M. Kaur, reversible watermarking techniques for medical images with ROI-temper detection and recovery - a survey, Int. J. Emerg. Technol.Adv. Eng. 2 (1) (2012) 32–36.
[2] J. Fridrich, M. Goljan, Lossless data embedding for all image formats, in: SPIE Proceedings of Photonics West, Electronic Imaging, Security and Watermarking of Multimedia Contents, 4675, 2002, pp. 572–583. San Jose
[3] Z. Zhang, H. Sun, S. Gao, S. Jin, Self-recovery reversible image watermarking algorithm, PloS ONE 13 (6) (2018) e0199143.
[4] N. Rashmi, K. Jyothi, "an improved method for reversible data hiding steganography combined with cryptography, in: IEEE on 2nd International Conference on Inventive Systems and Control (ICISC), 2018, pp. 81–84.
[5] D. Hou, W. Zhang, Y. Yang, N. Yu, Reversible data hiding under inconsistent distortion metrics, Trans. Image Process. 27 (10) (2018) 5087–5099.
[6] D. Hou, W. Zhang, J. Liu, S. Zhou, D. Chen, N. Yu, Emerging applications of reversible data hiding, Int. Conf. Image Graphics Process. (2019) 105–109.
[7] K. Chung, Y. Huang, P. Chang, H.M. Liao, Reversible data hiding-based approach for intra-frame error concealment in H.264/AVC, IEEE Trans. Circuits Syst. Video Technol. 20 (11) (2010) 1643–1647.
[8] Y.L. Chen, H. Wang, Y. Hu, A. Malik, Intra-frame error concealment scheme using 3d reversible data hiding in mobile cloud environment, IEEE Access 6 (2018) 77004–77013.
[9] A. Piva, F. Bartolini, M. Barni, Managing copyright in open networks, IEEE Internet Comput. 6 (3) (2002) 18–26.
[10] R.Y.M. Li, O.C. Au, C.K.M. Yuk, S.-K. Yip, T.-W. Chan, Enhanced image transcoding using reversible data hiding,", 2007, 1273–1276.
[11] K. Hwang, D. Li, Trusted cloud computing with secure resources and data coloring, IEEE Internet Comput. 5 (2010) 14–22.
[12] J. Tian, Reversible data embedding using a difference expansion, IEEE Trans. Circuits Syst. Video Technol. 13 (8) (2003) 890–896.
[13] A.M. Alattar, Reversible watermark using the difference expansion of a generalized integer transform, IEEE Trans. Image Process. 13 (8) (2004) 1147–1156.
[14] D. Thodi, J. Rodriguez, Expansion embedding techniques for reversible watermarking, IEEE Trans. Image Process. 16 (3) (2007) 721–730.
[15] V. Sachnev, H.J. Kim, J. Nam, S. Suresh, Y. Shi, Reversible watermarking algorithm using sorting and prediction, IEEE Trans. Circuits and Syst. Video Technol. 19 (7) (2009) 989–999.
[16] T.C. Lu, C.Y. Tseng, K.M. Deng, Reversible data hiding using local edge sensing prediction methods and adaptive thresholds, Signal Process. 104 (2014) 152–166.
[17] I. Dragoi, D. Coltuc, Local-prediction-based difference expansion reversible watermarking', IEEE Trans. Image Process. 23 (4) (2014) 1779–1790.
[18] B. Ou, X. Li, J. Wang, F. Peng, High-fidelity reversible data hiding based on geodesic path and pairwise prediction-error expansion, Neurocomputing 226 (2017) 23–34.
[19] S. Das, R. Maity, N.P. Maity, VLSI-based pipeline architecture for reversible image watermarking by difference expansion with high-level synthesis approach, Circuits Systems, and Signal Process. 37 (4) (2018) 1575–1593.
[20] Z. Ni, Y. Shi, N. Ansari, S. Wei, Reversible data hiding, IEEE Trans. Circuits Syst. Video Technol. 16 (3) (2006) 354–362.
[21] P. Tsai, Y.-C. Hu, H.L. Yeh, Reversible image hiding scheme using predictive coding and histogram shifting, Signal Process. 89 (3) (2009) 1129–1143.
[22] B. Ou, X. Li, Y. Zhao, R. Ni, Y. Shi, Pairwise prediction error expansion for efficient reversible data hiding, IEEE Trans. Image Process. 22 (12) (2013) 5010–5021.
[23] J. Wang, J. Ni, X. Zhang, Y. Shi, Rate and distortion optimization for reversible data hiding using multiple histogram shifting, IEEE Trans. Cybernetics. 47 (2) (2017) 315–326.
[24] S. Kim, X. Qu, V. Sachnev, Skewed histogram shifting for reversible data hiding using a pair of extreme predictions,", IEEE Trans. Circuits Syst. Video Technol. (2019). Online
[25] Y. Jia, Z. Yin, X. Zhang, Y. Luo, Reversible data hiding based on reducing invalid shifting of pixels in histogram shifting,", Signal Process. (2019). Online
[26] T. Kalker, F.M. Willems, Capacity bounds and code constructions for reversible data-hiding, 2002, 71–76.
[27] S. Lin, W. Chung, The scalar scheme for reversible information-embedding in gray-scale signals: capacity evaluation and code constructions, IEEE Trans. Inf. Forensics Secur. 7 (4) (2012) 1155–1167.
[28] X. Zhang, Reversible data hiding with optimal value transfer, IEEE Trans. Multimed. 15 (2) (2013) 316–325.
[29] W. Zhang, X. Hu, X. Li, N. Yu, Recursive histogram modification: Establishing equivalency between reversible data hiding and lossless data compression, IEEE Trans. Image Process. 22 (7) (2013) 2775–2785.
[30] X. Hu, W. Zhang, X. Hu, N. Yu, X. Zhao, F. Li, Fast estimation of optimal marked-signal distribution for reversible data hiding, IEEE Trans. Infor. Forensics Secur. 8 (5) (2013) 779–788.
[31] W. Zhang, X. Hu, X. Li, Y. Nenghai, Optimal transition probability of reversible data hiding for general distortion metrics and its applications, Trans. Image Process. 24 (1) (2015) 294–304.
[32] X.B. Ou, Y.Z. Li, R. Ni, Efficient color image reversible data hiding based on channel-dependent payload partition and adaptive embedding, Signal Process. 108 (2015) 642–657.
[33] D. Hou, W. Zhang, K. Chen, S. Lin, N. Yu, Reversible data hiding in color image with grayscale invariance, IEEE Trans. Circuits Syst. Video Technol. 29 (2) (2019) 363–374.
[34] E. Gao, Z. Pan, X. Gao, "adaptive embedding pattern for grayscale-invariance reversible data hiding, 2019, ArXiv preprint arXiv:1908.05965.
[35] M. Viola Paul, J. Jones, Robust real-time face detection, Int. J. Comput. Vis. 57 (2) (2004) 137–154.
[36] N. Dalal, B. Triggs, Histograms of oriented gradients for human detection, 2005, 886–893.
[37] D. Lowe, Distinctive image features from scale-invariant keypoints, Int. J. Comput. Vis. 60 (2) (2004) 91–110.
[38] C. Chang, C. Lin, Y. Fan, Lossless data hiding for color images based on block truncation coding, Pattern Recognit. 41 (7) (2008) 2347–2357.
[39] W. Yang, K. Chung, H. Liao, Efficient reversible data hiding for color filter array images, Inf. Sci. 190 (2012) 208–226.
[40] S. Dogan, A new data hiding method based on chaos embedded genetic algorithm for color image, Artif. Intell. Rev. 46 (1) (2016) 129–143.
[41] A. Nikolaidis, Low overhead reversible data hiding for color jpeg images, Multimedia Tools Appl. 75 (4) (2016) 1869–1881.
[42] H. Yao, C. Qin, Z. Tang, Y. Tian, Guided filtering based color image reversible data hiding, J. Vis. Commun. Image Represent. 43 (2017) 152–163.
[43] P. Singh, B. Raman, Reversible data hiding based on Shamirs secret sharing for color images over cloud, Inf. Sci. 422 (2018) 77–97.